International Journal of Minerals, Metallurgy and Materials
Volume 20, Number 10, October 2013, Page 953
DOI: 10.1007/s12613-013-0820-6

Hot deformation behavior of microstructural constituents in a duplex stainless steel during high-temperature straining

Amir Momeni[1)], *Shahab Kazemi*[2)], *and Ali Bahrani*[1)]

1) Materials Science and Engineering Department, Hamedan University of Technology, Hamedan 3733-1-65169, Iran

2) Department of Materials Engineering, Faculty of Engineering, Bu Ali Sina University, Hamedan 4161-65174, Iran

(Received: 05 January 2013; revised: 15 February 2013; accepted: 19 March 2013)

Abstract: The hot deformation characteristics of 1.4462 duplex stainless steel (DSS) were analyzed by considering strain partitioning between austenite and ferrite constituents. The individual behavior of ferrite and austenite in microstructure was studied in an iso-stress condition. Hot compression tests were performed at temperatures of 800-1100°C and strain rates of 0.001-1 s^{-1}. The flow stress was modeled by a hyperbolic sine constitutive equation, the corresponding constants and apparent activation energies were determined for the studied alloys. The constitutive equation and law of mixture were used to measure the contribution factor of each phase at any given strain. It is found that the contribution factor of ferrite exponentially declines as the Zener-Hollomon parameter (Z) increases. On the contrary, the austenite contribution polynomially increases with the increase of Z. At low Z values below $2.6.\times10^{15}$ ($\ln Z$=35.5), a negative contribution factor is determined for austenite that is attributed to dynamic recrystallization. At high Z values, the contribution factor of austenite is about two orders of magnitude greater than that of ferrite, and therefore, austenite can accommodate more strain. Microstructural characterization via electron back-scattered diffraction (EBSD) confirms the mechanical results and shows that austenite recrystallization is possible only at high temperature and low strain rate.

Keywords: duplex stainless steel; compression testing; strain partitioning; high temperature operations; deformation

1. Introduction

The high corrosion resistance and good strength characteristics of duplex stainless steels (DSS) have introduced them as deserving alternatives to the single-phase austenite and ferrite in different industries [1-4]. The coexistence of austenite and ferrite with different deformation responses in these alloys makes the processing complicated. It has been well understood that ferrite is characterized by high stacking fault energy (SFE) and is prone to dynamic recovery (DRV) [5-12]. On the other hand, austenite with low SFE undergoes the limited DRV but extensive dynamic recrystallization (DRX) [13-15].

Although the hot deformation behavior of duplex stainless steels has been investigated by many researchers, some controversies over restoration processes in microstructural constituents have still remained [4, 16-20]. It is known that the restoration behavior of austenite and ferrite in a duplex stainless steel are the same as that of single-phase materials. Albeit, the mutual influence of each other on different restoration processes has been controversial. It is known for certain that the coexistence of harder austenite and softer ferrite at high temperature leads to strain partitioning during hot deformation [21-26]. In this regard, even though some researches have been devoted to model the strain partitioning using the law of mixture, the real contribution of each constituent is still unclear [24]. Taking a general case, the different distributions of stress and strain in the constituents may cause very complicated state and hardly gives rise to the estimation of each phase contribution in total deformation. In the present investigation, a limiting condition of iso-stress was utilized to simplify the deformation behavior of such alloys at high temperature. The aim of this work was to study the behavior of each constituent and provide a good understanding and an acceptable estimation of the phase contribution.

Corresponding author: Amir Momeni E-mail: ammomeni@aut.ac.ir

2. Experimental

The material used in this study was 1.4462 duplex stainless steel with the composition of 0.025wt% C, 22.80wt% Cr, 5.20wt% Ni, 2.60wt% Mo, 0.30wt% Si, 1.50wt% Mn, 0.001wt% S, 0.025wt% P, 0.088wt% V, 0.23wt% Cu, 0.03wt% W, 0.068wt% Co, 0.028wt% Al, and the rest of Fe. Cylindrical specimens of 10 mm in diameter and 15 mm in height were machined from the as-received hot rolled plate so that the longitudinal axis of specimens was parallel to the rolling direction. Before testing, all the specimens were reheated to 1200°C, soaked for 5 min, and then subjected to continuous hot compression testing at temperatures of 800 to 1100°C and strain rates of 0.001 to 1 s^{-1} up to the true strain of 0.7. Graphite powders were applied on both contacting surfaces to reduce the friction coefficient during hot compression testing. To preserve the hot deformation microstructure, samples were immediately quenched after hot deformation. The hot deformed specimens were cut along the longitudinal axis and electrochemically polished. Microstructural characterization was carried out by electron back-scattered diffraction (EBSD) using a scanning electron microscopy (SEM, JEOL JSM-6500F) equipped with Channel 5 software.

To analyze the individual constitutive behavior of austenite and ferrite, the composition of each phase was determined by energy dispersive X-ray microanalysis (EDX). Two grades of ferritic and austenitic steels with the same analyzed compositions were produced using a vacuum induction furnace. The compositions of the produced single-phase ferritic and austenitic steels are shown in Table 1. Ingots were hot rolled at temperatures of 950°C and 1050°C for ferritic steel and austenitic steels, respectively. The 30-mm thick hot rolled specimens were then annealed at 1050°C followed by quenching in water. Similar to the studied DSS, hot compression samples of the produced ferritic and austenitic steels were tested under the same condition.

Table 1. Chemical composition of single-phase ferritic and austenitic stainless steels used in this investigation

wt%

Material	Cr	Ni	Mo	C	Mn	P	S	Si	Cu
Single-phase ferritic steel	25.80	3.31	2.68	0.02	0.4	0.018	0.010	0.35	0.3
Single-phase austenitic steel	20.09	8.78	2.33	0.03	2.8	0.033	0.001	0.26	0.16

3. Results and discussion

3.1. Flow curves and constitutive analysis

Fig. 1 demonstrates the typical flow curves of the studied DSS calculated from load-displacement data at different hot compression regimes. As it was mentioned earlier, to analyze the individual behavior of each constituent phase under hot working conditions, two single-phase ferritic and austenitic alloys were produced with the same chemical compositions as in the studied DSS. Fig. 2 exhibits the representative flow curves of the single-phase ferritic and austenitic alloys. The different apparent features of flow curves in Fig. 1 can be interpreted with regard to the coexistence of ferrite and austenite in the microstructure. As seen in Fig. 2, ferrite is prone to withstand DRV, while austenite is often softened by DRX [27]. As also expected, the flow stresses of ferrite and austenite increase with the decrease of temperature and the increase of strain rate. The flow curve of ferrite is characterized by a long plateau of steady-state deformation that reflects a dynamic balance between work hardening and flow softening due to DRV. In austenite, however, the limited potential for DRV causes work hardening to increase up to the peak flow stress, at which DRX comes into operation and softens the material.

The different apparent features of flow curves in Fig. 2 are directly due to different microstructural responses of ferrite and austenite to hot deformation. This is why the hot deformation behavior and thereby the flow curve characteristics of DSS significantly change by the different weight balance between ferrite and austenite at different deformation temperatures. It is evident that the flow curve of DSS is nearly typical of DRV at high temperature and low strain rate, where ferrite is the dominant component in microstructure. On the contrary, at low temperature or high strain rate, the flow curve turns to the typical form of DRX characterized by a work hardening stage up to a peak point and further flow softening.

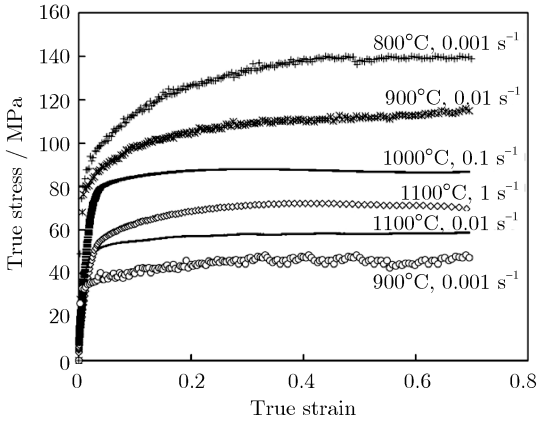

Fig. 1. Representative flow curves of the studied duplex stainless steel calculated from load-displacement data at different hot compression regimes.

In general, the coexistence of hard austenite and soft ferrite at high temperature results in strain partitioning

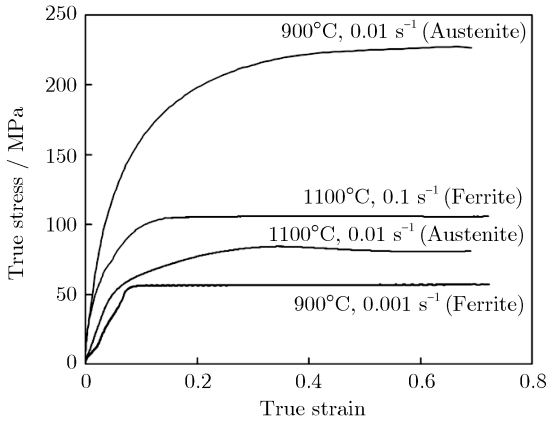

Fig. 2. Representative flow curves of the single-phase ferritic and austenitic alloys.

during hot straining. This is due to the fact that plastic deformation is first accommodated by the softer phase and then dominated by the harder one when the strain level is increased. The following law of mixture is often used to define the strain distribution between austenite and ferrite in a DSS.

$$\varepsilon_{\mathrm{DSS}} = F\varepsilon_{\mathrm{F}} + A\varepsilon_{\mathrm{A}} \tag{1}$$

where $\varepsilon_{\mathrm{DSS}}$, ε_{F}, and ε_{A} denote the strain of DSS, the strain accommodated by ferrite, and the strain accommodated by austenite, respectively; F and A indicate the contribution coefficients of ferrite and austenite, respectively. Some researchers [24] interpreted F and A as the volume fractions of ferrite and austenite constituents in the studied DSS, respectively. In the law of mixture, the material was considered as a composite, and the stress or strain was written as the sum of multiplied volume fraction of each phase by the corresponding strain or stress. It means that, e.g., for strain, $\varepsilon = \Sigma V_i \cdot \varepsilon_i$, so that ΣV_i=1. In the present paper, it is considered that not only the sum of volume fractions is equal unity, but also the sum of contribution factors should be tantamount to 1, which contains the effect of both volume fraction and deformation condition. This is necessary for the aggregate of two phases to work as a consistent composite material.

By differentiating from Eq. (1) with respect to deformation time, the following equation is given to correlate the strain rate of the studied DSS with those of each constituent.

$$\dot{\varepsilon}_{\mathrm{DSS}} = F\dot{\varepsilon}_{\mathrm{F}} + A\dot{\varepsilon}_{\mathrm{A}} \tag{2}$$

where $\dot{\varepsilon}_{\mathrm{DSS}}$, $\dot{\varepsilon}_{\mathrm{F}}$, and $\dot{\varepsilon}_{\mathrm{A}}$ denote the strain rate of DSS, the strain rate accommodated by ferrite, and the strain rate accommodated by austenite, respectively. F and A indicate the contribution coefficients of ferrite and austenite, respectively. Considering $F + A$=1, the values of F and A can be determined as

$$F = \frac{\dot{\varepsilon}_{\mathrm{DSS}} - \dot{\varepsilon}_{\mathrm{F}}}{\dot{\varepsilon}_{\mathrm{F}} - \dot{\varepsilon}_{\mathrm{A}}} \tag{3}$$

$$A = \frac{2\dot{\varepsilon}_{\mathrm{F}} - \dot{\varepsilon}_{\mathrm{A}} - \dot{\varepsilon}_{\mathrm{DSS}}}{\dot{\varepsilon}_{\mathrm{F}} - \dot{\varepsilon}_{\mathrm{A}}} \tag{4}$$

The next step to determine the incorporation coefficients of ferrite and austenite is to estimate the corresponding strain rates based on the given macroscopic strain rate. A hyperbolic sine constitutive equation proposed by Sellars and Tegart [28] is often used to describe the dependence of strain rate on stress and temperature under a hot working condition. This equation incorporated with the definition of Zener-Hollomon parameter is utilized to determine the strain rate of DSS as well as each constituent phase at any given deformation condition.

$$Z = \dot{\varepsilon} \cdot \exp\left(\frac{Q}{RT}\right) = A'[\sinh(\alpha \cdot \sigma)]^n \tag{5}$$

where Z is the Zener-Hollomon parameter, embracing the effects of strain rate and temperature, Q the hot deformation activation energy, T the temperature, R the gas constant (8.314472 J/mol·K), and A', α, and n the empirical material constants. The values of material constants for DSS and single-phase steel can be simply determined by fitting empirical data according to the following equation derived from Eq. (5).

$$\ln[\sinh(\alpha \cdot \sigma)] = \frac{1}{n}\left(\ln A' - \frac{Q}{RT}\right) + \frac{1}{n}\ln\dot{\varepsilon} \tag{6}$$

Fig. 3 indicates the variation of flow stress with strain rate and temperature at the typical strain of 0.5. By applying linear regression, the average slope of the left-hand graph stands for the value of $1/n$, and that of the right-hand graph indicates the value of Q/nR. The α value is determined as 0.012 and 0.014 for DSS and the single-phase alloys, respectively, so that the empirical lines become parallel. In a similar manner, Figs. 4 and 5 indicate the constitutive plots of empirical data for ferritic and austenitic steels, respectively. The high precision of fitted curves in Figs. 3-5 indicates that the adopted constitutive equation can be used to model the strain rate of constituents in the studied DSS.

Fig. 6 exhibits the variation of flow stress with Z parameter, the intercept of each curve gives the A' value according to Eq. (5). This figure also emphasizes that the flow stress of DSS is actually the average of the single-phase ferritic and austenitic alloy. By replacing the calculated constants in the constitutive equation, the strain rates of DSS, ferritic, and austenitic stainless steels can be calculated using the following equations.

$$\dot{\varepsilon}_{\mathrm{DSS}} = 2 \times 10^{16}[\sinh(0.012\sigma)]^{4.2}\exp\left(\frac{432000}{8.314T}\right) \tag{7}$$

$$\dot{\varepsilon}_{\mathrm{F}} = 1.42 \times 10^{12}[\sinh(0.014\sigma)]^{4.61}\exp\left(\frac{334000}{8.314T}\right) \tag{8}$$

$$\dot{\varepsilon}_{\mathrm{A}} = 2 \times 10^{19}[\sinh(0.014\sigma)]^{4.31}\exp\left(\frac{570000}{8.314T}\right) \tag{9}$$

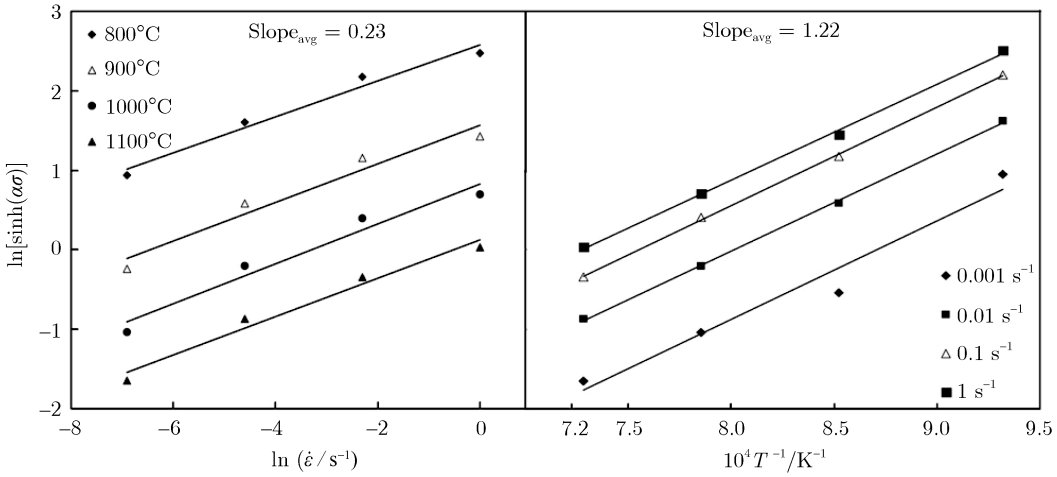

Fig. 3. Variation in flow stress of the studied DSS at the typical strain of 0.5 with strain rate and temperature according to the hyperbolic sine constitutive equation.

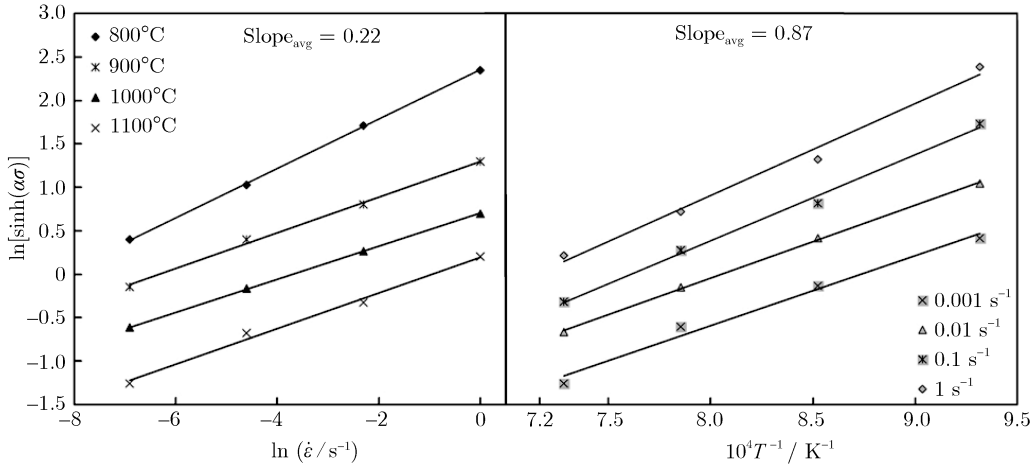

Fig. 4. Variation in flow stress of the single-phase ferritic stainless steel at the typical strain of 0.5 with strain rate and temperature according to the hyperbolic sine constitutive equation.

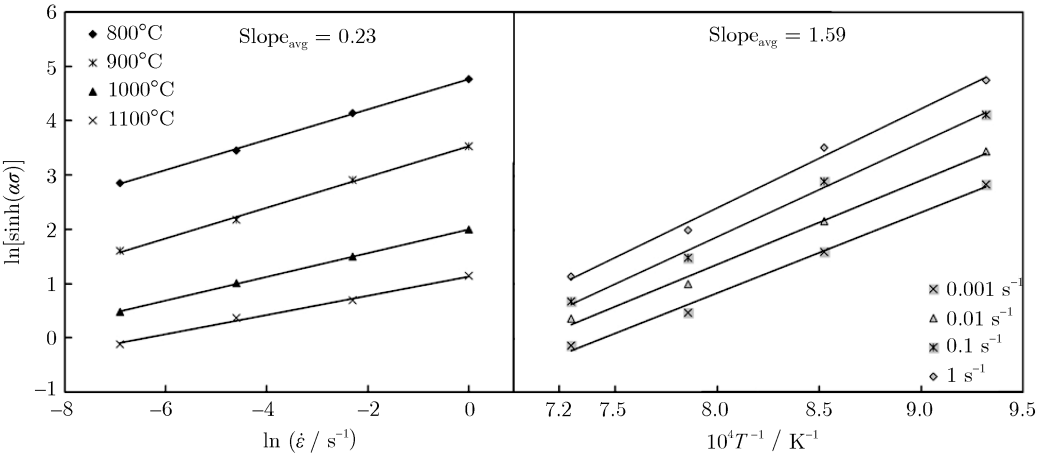

Fig. 5. Variation in flow stress of the single-phase austenitic stainless steel at the typical strain of 0.5 with strain rate and temperature according to the hyperbolic sine constitutive equation.

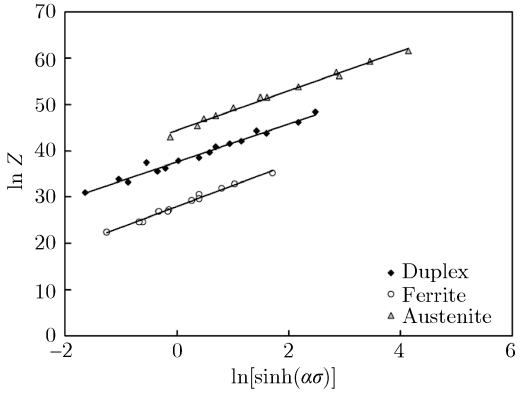

Fig. 6. Hyperbolic sine functions of flow stress with Zener-Hollomon parameter for the studied DSS, single phase ferritic and single phase austenitic alloys.

The strain rate of the studied DSS, ferritic, and austenitic alloys can be calculated using Eqs. (7)-(9). Therefore, it is possible to calculate the F and A values using Eqs. (3) and (4) at different deformation conditions.

Figs. 7 and 8 indicate the variation of F and A with Z parameter at a strain of 0.5, respectively. As expected, the contribution factor of ferrite, F, declines as Z parameter increases. As a matter of fact, when the deformation temperature decreases and/or strain rate increases, DRV in ferrite slows down, therefore the strain distribution to austenite takes place more rapidly. This, in turn, reduces the contribution of ferrite in the total applied strain. On the other hand, the polynomial increase of A with Z suggests more contribution of austenite in total strain at higher strain rates and lower temperatures. In fact, at high Z values, when the stated DRV in ferrite is sluggish, strain is more accommodated by austenite which has a higher work hardening capacity.

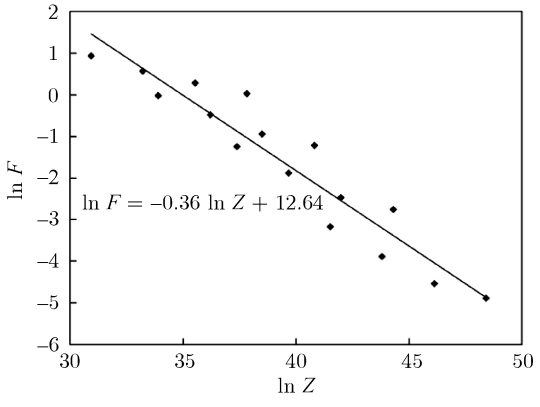

Fig. 7. Contribution factor of ferrite (F) as a function of Zener-Hollomon parameter at the typical strain of 0.5.

Fig. 8 introduces three regions of A as dependent on the Z value. The first region is characterized by the negative values of A. According to the mathematical expressions of A and F by Eqs. (1) and (2), they should be positive. However, from the phenomenological point of view, the negative value of A can be attributed to the occurrence of DRX in austenite that gives rise to the decrease of flow stress and accumulates strain in this phase. The results show that at low Z values ($\ln Z<35.5$), corresponding to high deformation temperatures and low strain rates, the negative values of A can be associated with DRX in austenite. The proposed idea can be exemplified by the flow curves of single-phase austenitic steel obtained at 900°C, 0.01 s^{-1} and 1100°C, 0.01s^{-1}, as shown in Fig. 2. Although the former flow curve with $\ln Z$=39.7 exhibits the work hardening of austenite, the latter flow curve with $\ln Z$=33.2 indicates flow softening due to DRX at the strain of 0.5.

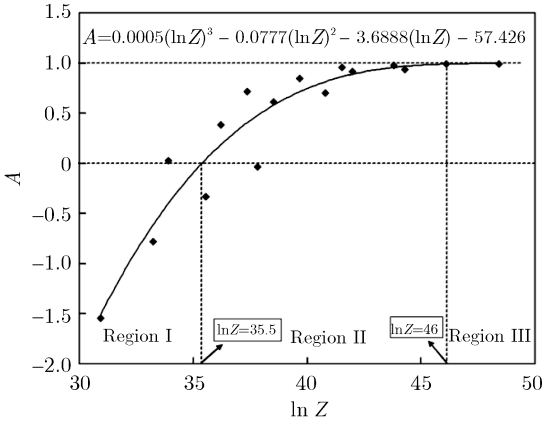

Fig. 8. Contribution factor of austenite (A) as a function of Zener-Hollomon parameter at the typical strain of 0.5.

At higher Z values, region II, the contribution factor of austenite increases as Z rises, and that of ferrite decreases. In this region, a weighted average of austenite and ferrite contributions governs the deformation behavior. Over a critical Z value ($\ln Z>$ 46), the contribution factor of austenite (A) is nearly equal to unity, and that of ferrite (F) is as low as 0.01. In this case, which is associated with low temperature and high strain rate, most of the applied strain is accommodated by austenite. However, although in this condition, DRV in ferrite is still working, but austenite is work hardened, and DRX is pushed to very high strain levels. The low tendency for DRX in austenite in this region can be attributed to the different reasons. The first reason is that, the driving force for the nucleation of DRX at low temperature and high strain rate is very low. The second reason is that, there are very few grain boundaries inside the highly elongated austenite strings to act as the source of DRX nuclei. In addition, DRX cannot nucleate at the immobile austenite-ferrite interphase boundaries [12].

3.2. Microstructural characterization

The EBSD analysis of hot deformed samples was performed to verify the results of mechanical testing. Fig. 9 shows the microstructures of deformed samples at the strain rate of 0.01 s^{-1} and the temperatures of 900°C and 1100°C. As mentioned, at 900°C and 0.01 s^{-1}, ln$Z$ is equal to 39.7, and A is located in the second region in Fig. 8. At this condition of low temperature and medium strain rate, A is obtained about 0.7, and therefore, the value of F is about 0.3. This indicates that most of strain is accommodated by austenite, as shown in Fig. 2, DRX is impossible at the strain of 0.5. Consistent with these anticipations, Fig. 9(a) indicates the elongated austenite islands in the ferritic matrix that is characterized by small equiaxial grains. Boundaries highlighted by red color are Σ3 type boundaries. Equiaxed grains observed in ferrite phase indicate the occurrence of DRV even at low temperature, corresponding to low contribution factor. Besides, the low density of high angle boundaries in austenitic islands reflects low DRX. At 1100°C and 0.01 s^{-1} in Fig. 9(b), the austenitic islands are more globular with the higher density of high angle and Σ3 boundaries, which are associated with a higher DRX in this phase. As mentioned, the regime of 1100°C and 0.01 s^{-1} is located in the first region in Fig. 9, and the mechanical testing predicts DRX in austenite.

Fig. 10 indicates how the microstructure of DSS is af-

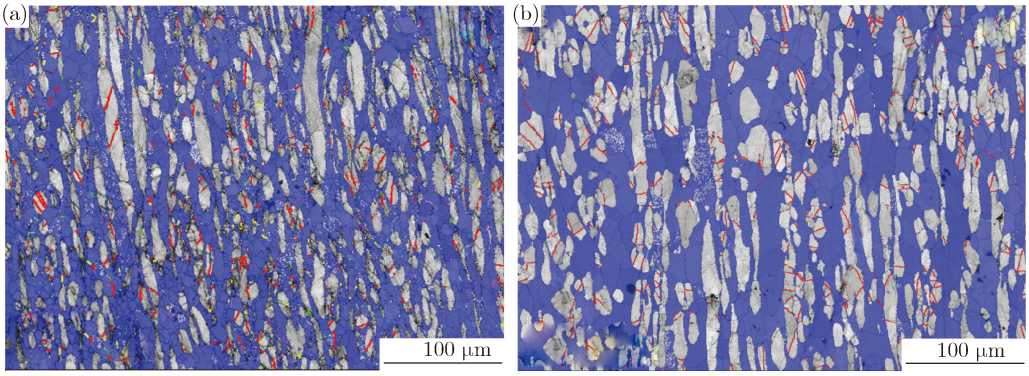

Fig. 9. EBSD micrographs of hot deformed samples at the strain rate of 0.01 s^{-1} and the temperatures of 900°C (a) and 1100°C (b).

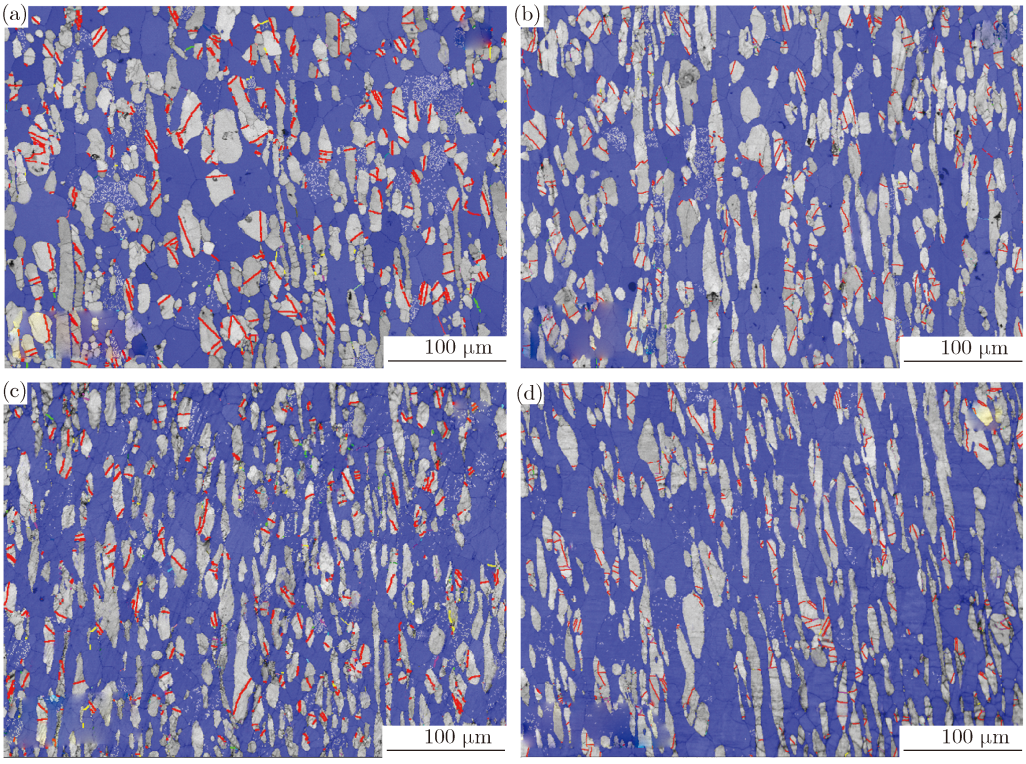

Fig. 10. EBSD micrographs of hot deformed samples at the temperature of 1100°C and the strain rates of 0.001 s^{-1} (a), 0.01 s^{-1} (b), 0.1 s^{-1} (c), and 1 s^{-1} (d).

fected by the change of strain rate. Obviously, the increase of strain rate has no considerable influence on the ferritic matrix, and the equiaxed grains are observed even at 1 s^{-1} in Fig. 10(d). However, the average grain size in the ferritic matrix decreases with the increase of strain rate due to the shrinking influence of a higher flow stress on subgrain size. In austenite islands, special attention should be paid to the variation of morphology and the change of density in common high angle and $\Sigma 3$ boundaries. Increasing the strain rate particularly leads to more elongated austenite islands; however, the strain value is constant. This indicates that at low strain rate, the applied strain is accommodated by two terms: firstly, the change in morphology of austenite to globular islands; and secondly, the microstructural change through DRX. At higher strain rates, actually beyond 0.001 s^{-1}, austenitic islands cannot comply with higher rates of deformation, and therefore considerably elongates. On the other hand, higher strain rates push the start of DRX to higher strains, and consequently, austenite remains elongated and unrecrystallized over the common strain values that are adopted during hot compression. Decreasing the density of high angle grain boundaries (red lines in Fig. 10) with the increase of strain rate implies that the tendency of DRX in austenite decreases as the strain rate rises. These results are consistent with results in Figs. 7 and 8, when $\ln Z$ is calculated as 30.9, 33.2, 35.5, and 37.8 for the strain rates of 0.001 s^{-1}, 0.01 s^{-1}, 0.1 s^{-1}, and 1 s^{-1}, respectively.

4. Conclusions

(1) Flow curves of the studied duplex stainless steel at low temperature, where austenite is the dominant component in microstructure, is characterized by a faint peak, which is similar to the DRX flow curves. Whereas at high temperature, ferrite is the dominant phase, the flow curves resemble the DRV curves.

(2) The hyperbolic sine constitutive equations of DSS, ferritic, and austenitic stainless steels are determined and used to calculate the strain rate of constituents in the structure of the studied duplex steel.

(3) Under the iso-stress condition between the constituents, the contribution factor of each phase to the total strain is determined using the law of mixture.

(4) It is found that the contribution factor of ferrite exponentially decreases as Z increases. Otherwise, the austenite contribution factor increases with Z, according to a polynomial trend.

(5) At low Z values, $\ln Z < 35.5$, the austenite contribution factor is negative. It is attributed to the occurrence of DRX in this phase. On the other hand, at high Z values, $\ln Z > 46$, the austenite contribution factor is nearly equal to 1. EBSD analyses of deformed samples corroborates the mechanical results.

References

[1] A. Itman Filho, J.M.D.A. Rollo, R.V. Silva, and G. Martinez, Alternative process to manufacture austenitic-ferritic stainless steel wires, *Mater. Lett.*, 59(2005), No. 10, p. 1192.

[2] I. Gurrappa and C.V. Krishna Reddy, Characterization of newly developed structural DMR-1700 steel and comparison with different steels for chemical applications, *J. Mater. Process. Technol.*, 182(2007), p. 195.

[3] C.M. Garzón and A.P. Tschiptschin, EBSD texture analysis of a high temperature gas nitrided duplex stainless steel, *Mater. Sci. Eng. A*, 441(2006), No. 1-2, p. 230.

[4] J.M. Cabrera, A. Mateo, L. Llanes, J.M. Prado, and M. Anglada, Hot deformation of duplex stainless steels, *J. Mater. Process. Technol.,* 143-144(2003), p. 321.

[5] H.J. McQueen and D.L. Bourell, *Formability and Metallurgical Structure*, Edited by A.K. Sachdev and J.D. Embury, TMS, Warrendale, 1986, p. 341.

[6] C. Huang, *Flow Stress, Restoration and Precipitation Behavior, and Modeling for Two Ti-Nb Stabilized IF Steels in the Ferrite Region* [Dissertation], University of British Columbia, Canada, 1999.

[7] H.J. McQueen, N.D. Ryan, E. Evangelista, and X. Xia, Flow stresses, grain and subgrain structures developed by hot working in as-cast 409 stainless steel, [in] *Proceedings of the 34th Mechanical Working Steel Processing Conference*, Iron and Steel Society of AIME, Warrendale, 1993, p. 101.

[8] G.S. Reis, A.M. Jorge Jr., and O. Balancin, Influence of the microstructure of duplex stainless steels on their failure characteristics during hot deformation, *Mater. Res.*, 3(2000), No. 2, p. 31.

[9] E. Evangelista, H.J. McQueen, B. Verlinden, and M. Barteri, Hot forming of duplex stainless steels, [in] *Proceedings of the* 3*rd European Congress "Stainless Steels '99 – Science and Market"*, Milano, 1999, p. 253.

[10] F. Tehovnik, B. Arzenšek, B. Arh, D. Skobir, B. Pirnar, and B. Žužek, Microstructure evolution in SAF 2507 super duplex stainless steel, *Mater. Technol.*, 45(2011), No. 4, p. 339.

[11] P.L. Mao, K. Yang, and G.Y. Su, Hot deformation behavior of an as-cast duplex stainless steel, *J. Mater. Sci. Technol.*, 19(2003), No. 4, p. 379.

[12] E. Evangelista, H.J. McQueen, M. Niewczas, and M. Cabibbo, Hot workability of 2304 and 2205 duplex stainless steels, *Can. Metall. Q.*, 43(2004), No. 3, p. 339.

[13] A. Momeni, S.M. Abbasi, and A. Shokuhfar, Hot compression behavior of as-cast precipitation-hardening stainless steel, *J. Iron Steel Res. Int.*, 14(2007), No. 5, p. 66.

[14] A. Momeni, A. Shokuhfar, and S.M. Abbasi, Dynamic recrystallization of a Cr-Ni-Mo-Cu-Ti-V precipitation hardenable stainless steel, *J. Mater. Sci. Technol.*, 23(2007),

p. 775.

[15] M.S. Chen, Y.C. Lin, and X.S. Ma, The kinetics of dynamic recrystallization of 42CrMo steel, *Mater. Sci. Eng. A*, 556(2012), p. 260.

[16] G. Niewielski, K. Radwański, and D. Kuc, The influence of hot-working processing on plasticity and structure of duplex steel, *Arch. Mater. Sci. Eng.*, 28(2007), No. 6, p. 325.

[17] P. Cizek, B.P. Wynne, and W.M. Rainforth, EBSD investigation of the effect of strain path changes on the microstructure and texture of duplex stainless steel during hot deformation, *J. Phys. Conf. Ser.*, 26(2006), p. 331.

[18] H. Farnoush, A. Momeni, K. Dehghani, J. Aghazadeh Mohandesi, and H. Keshmiri, Hot deformation characteristics of 2205 duplex stainless steel based on the behavior of constituent phases, *Mater. Des.*, 31(2010), p. 220.

[19] L.E. Hernandez-Castillo, J.H. Beynon, C. Pinna, and S. Van Der Zwaag, Micro-scale strain distribution in hot-worked duplex stainless steel, *Steel Res. Int.*, 76(2005), No. 2-3, p. 137.

[20] A. Dehghan-Manshadi and P.D. Hodgson, Effect of δ-ferrite co-existence on hot deformation and recrystallization of austenite, *J. Mater. Sci.*, 43(2008), No. 18, p. 6272.

[21] A. Momeni, K. Dehghani, and X.X. Zhang, Mechanical and microstructural analysis of 2205 duplex stainless steel under hot working condition, *J. Mater. Sci.*, 47(2012), p. 2966.

[22] L. Duprez, B.C. De Cooman, and N. Akdut, High-temperature stress and strain partitioning in duplex stainless steel, *Z. Metallkd.*, 93(2002) p. 236.

[23] J. Johansson and M. Odén, Load sharing between austenite and ferrite in a duplex stainless steel during cyclic loading, *Metall. Mater. Trans. A*, 31(2000), p. 1557.

[24] A. Iza-Mendia, A. Piñol-Juez, J.J. Urcola, and I. Gutierrez, Microstructural and mechanical behavior of a duplex stainless steel under hot working conditions, *Metall. Mater. Trans. A*, 29(1998), p. 2975.

[25] O. Balancin, W.A.M. Hoffmann, and J.J. Jonas, Influence of microstructure on the flow behavior of duplex stainless steels at high temperatures, *Metall. Mater. Trans. A*, 31(2000), p. 1353.

[26] L. Duprez, B.C. De Cooman, and N. Akdut, Flow stress and ductility of duplex stainless steel during high-temperature torsion deformation, *Metall. Mater. Trans. A*, 33(2002), p. 1931.

[27] Y.C. Lin and X.M. Chen. A critical review of experimental results and constitutive descriptions for metals and alloys in hot working, *Mater. Des.*, 32(2011), p. 1733.

[28] C.M. Sellars and W.J. McG. Tegart, Hot workability, *Int. Mater. Rev.*, 17(1972), No. 1, p. 1.